Available online at www.CivileJournal.org

Civil Engineering Journal

(E-ISSN: 2476-3055; ISSN: 2676-6957)

Vol. 12, No. 03, March, 2026

Investigation of Slit Link Behavior with Wide-Flange (WF) Sections in Eccentrically Braced Frames (EBFs)

Jusuf Wilson Meynerd Rafael [1], Budi Suswanto [1*], Chien-Kuo Chiu [1, 2], Data Iranata [1], Aniendhita R. Amalia [1], Fikri Ghifari [2]

[1] *Department of Civil Engineering, Institut Teknologi Sepuluh Nopember, Surabaya 60111, Indonesia.*

[2] *Department of Civil and Construction Engineering, National Taiwan University of Science and Technology, Taipei 10607, Taiwan.*

Received 03 December 2025; Revised 15 February 2026; Accepted 22 February 2026; Published 01 March 2026

Abstract

This study investigates the seismic performance of slit link configurations using wide-flange (WF) sections within eccentrically braced frames (EBFs), addressing the limited application of slit geometries in practical steel construction. The objective is to evaluate the influence of slit shape and width on shear strength, ductility, and energy dissipation, while ensuring damage localization within the link element. Six analytical models were developed, including conventional links (CV and CV-ST) and slit variants (SL-1 to SL-4), and analyzed through nonlinear finite element simulations in ABAQUS under the AISC 341-22 cyclic loading protocol. The analysis focused on stress distribution, hysteretic response, backbone curve stability, and energy dissipation. Results show that conventional links provide higher peak shear strength and energy absorption but transmit stresses into adjacent members, increasing repair complexity. In contrast, slit links confine plastic deformation within the link region, enhancing ductility and repairability at the expense of reduced strength. Among the slit variants, the parabolic slit (SL-4) demonstrated smoother stress redistribution and improved cyclic stability compared to rectangular slits. The novelty of this research lies in embedding slit geometries directly into WF profiles, offering a cost-effective fuse mechanism that bridges theoretical slit damper concepts with real-world EBF applications.

Keywords: Slit Link; Wide-Flange; Ductility; Energy Dissipation; Seismic Performance.

1. Introduction

As a hybrid of the Moment Resisting Frame (MRFs) and the Concentrically Braced Frame (CBFs) systems, the Eccentrically Braced Frame (EBFs) provides significant advantages in terms of elastic stiffness and energy dissipation [1-3]. In the EBFs configuration, at least one end of each bracing member is connected eccentrically to the frame, thereby forming a link element that plays a critical role in seismic performance [4, 5]. The link element (e), as illustrated in Figure 1 [6], is the structural component of the EBF that is intentionally allowed to sustain damage during seismic events. This occurs as a result of lateral forces that induce moment and shear concentration within the link [7]. Consequently, yielding is confined to the link, while the other structural components—such as the outer beams, columns, and bracing—are proportioned to remain elastic [8, 9]. This scenario arises when the link functions as a short beam subjected to opposing shear stresses at each end [10, 11], as depicted in Figure 2 [12].

* Corresponding author: budi_suswanto@its.ac.id

https://doi.org/10.28991/CEJ-2026-012-03-08

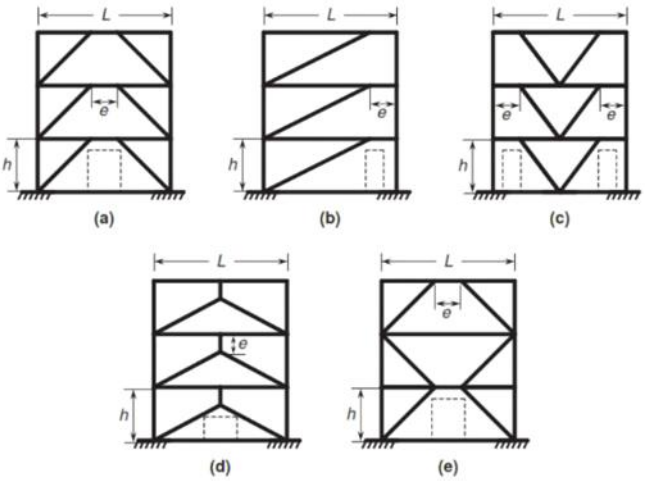

Figure 1. EBFs configuration: (a) K-braces, (b) V-braces, (c) Inverted Y-braces, (d) K-braces & Inverted K-braces [6]

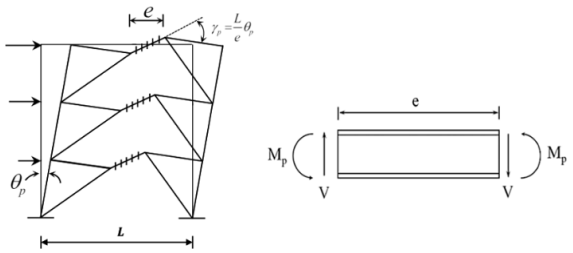

(a) (b)

Figure 2. (a) Plastic rotation angle of the link, (b) Forces in an isolated link [12]

Although the link element is intentionally permitted to sustain damage following an earthquake, such damage often extends to other structural components, including beams outside the link, columns, and diagonal bracing [13], as illustrated in Figure 3 [9, 14]. Damage to structural elements beyond the link is undesirable, as it complicates repair efforts and inevitably increases both cost and time requirements. Consequently, the development of link beams—whether through variations in link geometry or through improved connection systems between the link beam, the surrounding beams, and the bracing—has become a central focus of current research. The design of link beams must ensure adequate ductility and energy dissipation capacity while avoiding concentrations of inelastic stresses in regions outside the link beam component, consistent with the concept of steel slit dampers (SSD) as the slit links.

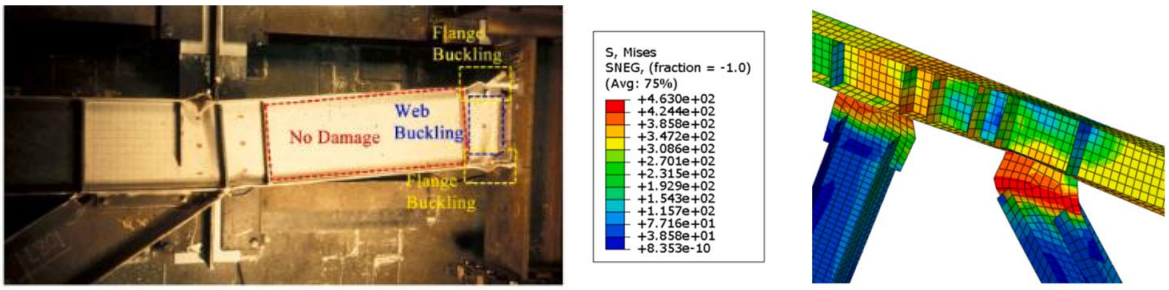

(a) (b)

Figure 3. Link failure modes affecting (a) the beams outside the link [9], (b) the diagonal bracing [14]

Steel Slit Dampers (SSD), as illustrated in Figure 4 [15], represent a specific type of Metallic Yielding Dampers (MYD) formed by introducing slits or openings into steel plates that undergo shear deformation along the beam plane [15]. These slits divide the plate into multiple links, which dissipate input energy through plastic deformation across the plate surface [16, 17]. Through the overall shear deformation of the plate, these links act in parallel, exhibiting combined flexural and shear behavior. In a well-designed structural system equipped with passive control devices, dampers must be engineered to dissipate hysteretic energy and prevent significant nonlinear deformations in the primary structural members [18, 19]. In other words, during strong earthquakes, these devices function as fuses, preventing failure, damage, or even excessive deformation in the main structural components—such as beams outside the link, columns, and bracing—thus ensuring that these elements remain functional after seismic events. However, the shape/pattern of the slits, the thickness of the slit damper plates, and the position/placement of the slit dampers all have a significant impact on the energy dissipation and performance produced. Consequently, numerous recommendations for slit link models have been made to date.

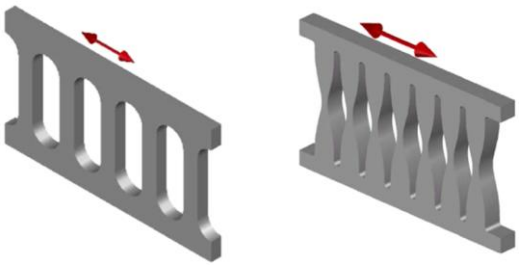

(a) (b)

Figure 4. Slit damper with (a) block slit (b) parabolic slit [15]

The application of Steel Slit Dampers (SSD) as slit links in Eccentrically Braced Frames (EBF), in the form of block slit dampers, has been investigated by Mohseni et al. (2020) [20], Amiri et al. (2020) [21], Oh & Park (2022) [22], Hwang et al. (2023) [23], and Zhou et al. (2025) [24]. Similarly, the use of parabolic slit dampers has been examined by Askariani et al. (2020) [25], Montazeri et al. (2021) [26], and Suswanto et al. (2025) [27]. The findings of these investigations demonstrate that slit link configurations exhibit superior seismic performance compared to conventional link models. Block slits of varying widths alter the effective shear area, reducing shear capacity but confining damage. Parabolic slits, by contrast, smooth stress distribution and reduce concentration at slit tips, potentially improving cycle stability. Despite these advances, the integration of slit geometries directly into EBF link beams remains limited. Most prior studies have focused on slit dampers as separate devices rather than as modifications of the link itself. Embedding slits into the web of the link beam offers the potential to create a "fuse" mechanism that localizes damage while maintaining global frame stability.

A notable gap in the literature is the choice of section type for slit links. Many studies have adopted built up plate sections—such as welded box or stiffened plate links—because they offer superior lateral torsional stability and allow flexible slit arrangements [28, 29]. Built up sections are easier to customize but require additional fabrication effort. In contrast, Wide-Flange (WF) sections are widely available, economical, and commonly used in practice. However, slit link applications using WF profiles have been scarcely investigated. The majority of slit damper research assumes built up geometries, leaving a knowledge gap regarding the performance of standard WF sections with slits introduced into their webs. The absence of systematic investigations on WF slit links limits their adoption in design practice. From a practical standpoint, WF sections are attractive because they are standardized, readily available in structural steel catalogs, and widely used in Indonesian and international construction. Introducing slits into WF webs could provide a cost-effective alternative to custom built up dampers, aligning with performance based seismic design principles.

Therefore, this study proposes a systematic investigation of slit links embedded in WF profiles. Six EBFs models—conventional, stiffened, and slit variants—are analyzed using nonlinear finite element simulations in Abaqus under the AISC 341 22 cyclic protocol. The focus is on quantifying shear capacity, hysteretic stability, degradation metrics, and stress localization. By addressing the underexplored area of WF slit links, this research contributes to bridging the gap between theoretical slit damper concepts and practical EBF applications. The findings aim to demonstrate that WF slit links can serve as economical, reparable fuse elements, offering a balance between strength, ductility, and post-earthquake resilience.

2. Research Significance

This study aims to address this research gap by performing a numerical analysis on a slit link using WF profiles with block slit and parabolic slit configurations. This research highlights the behavior of slit links under various loading conditions. The parameters analyzed include slit shape configuration, opening width, and cyclic loading based on AISC 341-22. For comparison, simulations were also conducted on a conventional link model to observe their significant impact on EBFs performance. The connections between structural components were assumed to be welded joints to examine the stress distribution to components outside the link beam. Numerical analysis was performed using the finite element method (FEM) implemented thru ABAQUS software, enabling accurate simulation of nonlinear material and structural behavior. This approach yields a numerical model that represents the slit link's response with a WF profile, including strength, energy dissipation, deformation, and stress distribution under cyclic loading. This study aims to provide a more comprehensive understanding of the performance of slit links with WF profiles and simultaneously serve as a valuable reference for developing more optimal slit link designs for earthquake-resistant building structures. Figure 5 shows an illustration of the research flowchart.

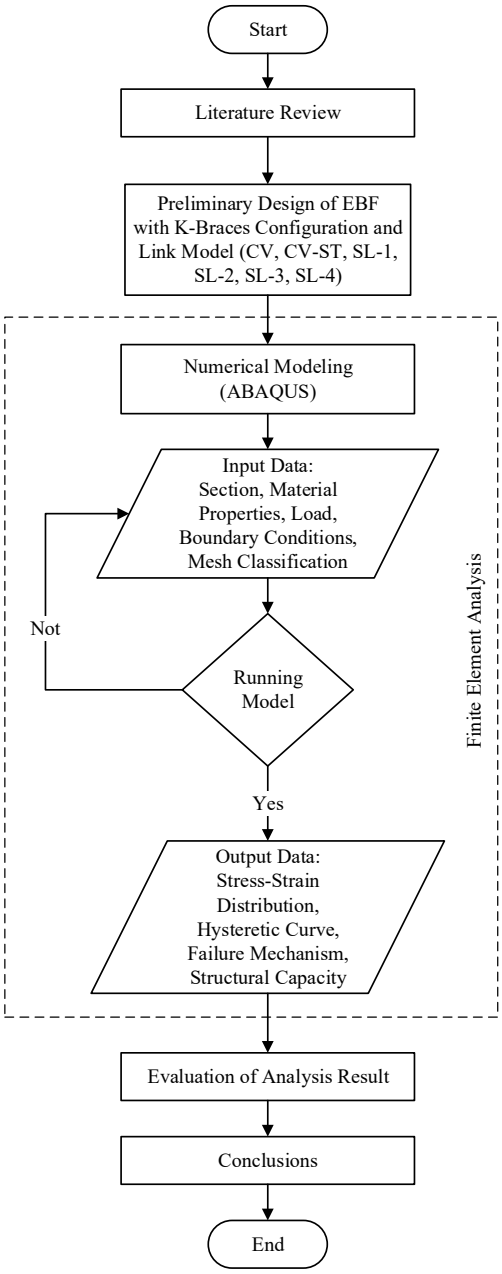

Figure 5. The research flowchart

3. Method of Research

3.1. Materials and Steel Section

The steel grade of the link beam is same with the beam outside the link, columns and bracing, ASTM-A36 with the yield strength of 245 MPa and ultimate tensile strength of 470 MPa. The link, beam outside the link and column used Wide-Flange (WF) profile, and bracing used H profile. Detailed of the material properties and frame section shown on Table 1 and Tabel 2.

Table 1. Material properties of ASTM-A36

Property	Value
f_y (in MPa)	245
f_u (in MPa)	470
E_s (in MPa)	210,000
Density (in kg/m^3)	7,850
e_{max} (in %)	16
Poisson's ratio	0.3

Table 2. The steel section of EBFs

No.	Links Configuration	Column	Beam	Link	Bracing
1	CV	WF588×300×12×20	WF588×300×12×20	WF588×300×12×20	H300×30015×15
2	CV-ST	WF588×300×12×20	WF588×300×12×20	WF588×300×12×20	H300×30015×15
3	SL-1	WF588×300×12×20	WF588×300×12×20	WF588×300×12×20	H300×30015×15
4	SL-2	WF588×300×12×20	WF588×300×12×20	WF588×300×12×20	H300×30015×15
5	SL-3	WF588×300×12×20	WF588×300×12×20	WF588×300×12×20	H300×30015×15
6	SL-4	WF588×300×12×20	WF588×300×12×20	WF588×300×12×20	H300×30015×15

3.2. The Length of the Links

The steel grade This study investigates the K-braced Eccentrically Braced Frame (K-EBF) system utilizing wide flange (WF) link elements. The horizontal link located at mid-span connects the main beam to the bracing and serves as the primary energy-dissipating component of the system. To evaluate seismic performance and energy dissipation efficiency, a short-link approach was adopted. The link length (e) is determined based on the ratio (ρ) of the plastic moment capacity (M_P) to the plastic shear capacity (V_P), calculated according to the link cross-section properties and expressed in Equation 1 [30]. The plastic moment capacity (M_P) and plastic shear capacity (V_P) are obtained using Equation 2 and Equation 3 [31]. A ratio value less than 1.6 is classified as a short link, whereas a ratio greater than 2.6 is categorized as a long link [32]. Accordingly, the link lengths employed in this study are presented in Table 3 with a ratio of 1.37 for a length of 1500 mm, categorized as short links.

$$\rho = \frac{e}{M_P / V_P} \tag{1}$$

$$M_P = Z_x f_y \tag{2}$$

$$V_P = 0.6 f_y (d - 2t_f) t_w \tag{3}$$

Table 3. The link lengths calculation for WF 588.300.12.20 section

e (mm)	d (mm)	t_w (mm)	t_f (mm)	Z_x (mm³)	f_y (MPa)	V_P (N)	M_P (N.mm)	ρ
1,500	588	12	20	4,308,912	245	966,672	1,055,683,440	1.37

The introduction of slits into the web of WF section does not alter the global link length or the overall classification; however, it does create localized regions of compliance that slightly modify the effective shear length. This effect manifests as localized increases in the M_P/V_P ratio near the slit edges, while the global classification as short links remains valid. Thus, the slit links can still be evaluated within the framework of standard EBF link classifications, with the caveat that local stress redistribution must be considered in interpreting their cyclic performance.

3.3. Links Configuration

In this study, six analytical models with variations in slit geometry and configuration are used. The first model of link, CV (Conventional Vertical link), represents a standard WF link without geometric modification. The second model, CV-ST (Conventional Vertical link with Stiffener), is an enhanced version of CV, incorporating transverse stiffeners to improve shear capacity and mitigate local deformation. The remaining four models consist of slit link configurations, designed to enhance ductility and energy dissipation through controlled plastic deformation mechanisms. Specifically, SL-1, SL-2, and SL-3 adopt block-slit geometries modified from Hwang et al. (2023) [23], with varying slit widths to examine the influence of opening ratios on hysteretic capacity. Meanwhile, SL-4 employs a parabolic-slit geometry, adapted and modified from Askariani et al. (2020) [25], to achieve a more uniform distribution of plastic strains along the link length. All models were analyzed using finite element simulations to assess structural response under seismic loading. The analysis focused on key performance parameters, including ductility, shear strength, and energy dissipation. Comparative evaluation among the six models was conducted to identify the most effective slit link configuration for improving the seismic performance of K-EBF systems. The proposed slit link geometries are illustrated in Figure 6.

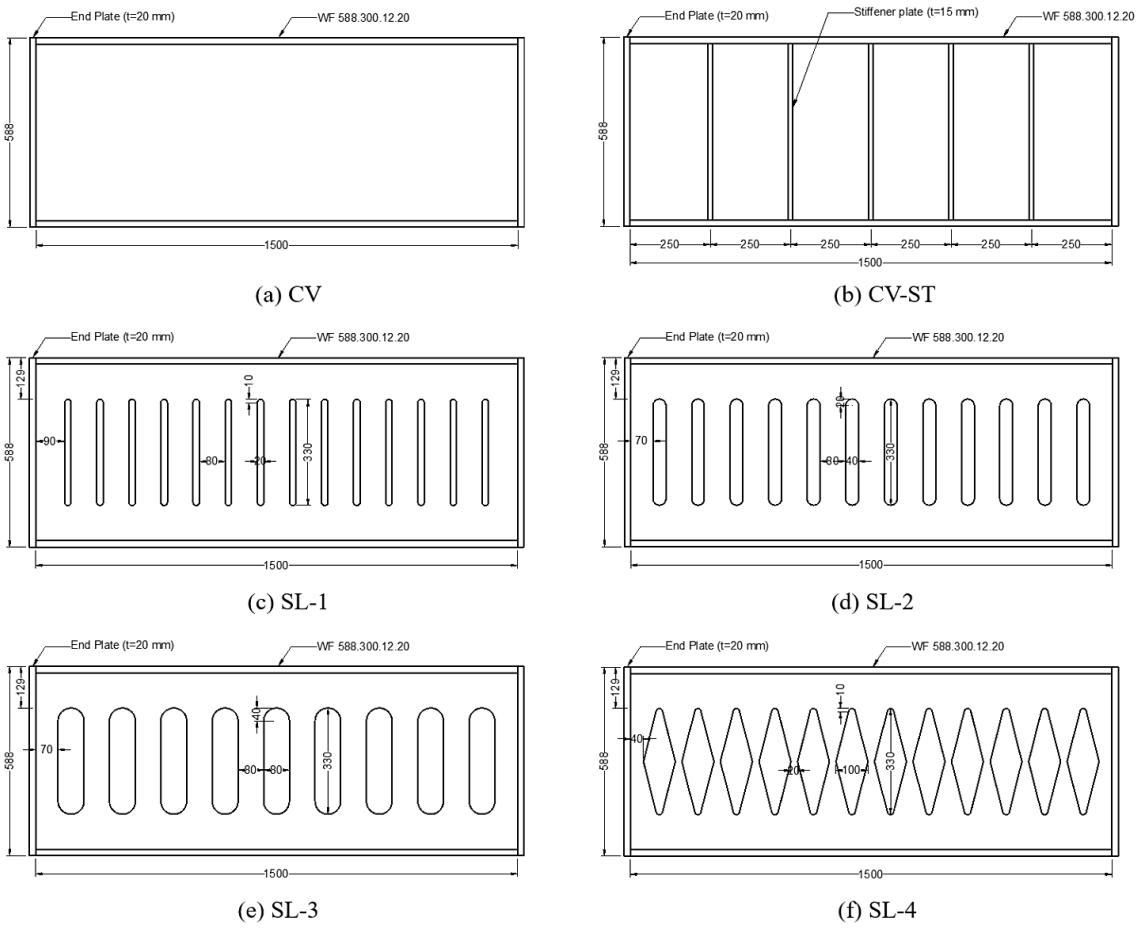

Figure 6. The proposed slink link geometries (unit in mm)

3.4. Modeling and Loading Protocol

The analysis of the slit link in the EBFs was conducted using the finite element method thru the ABAQUS software. The selection of the cross-section dimensions was first determined thru structural analysis to verify that the strength of the EBFs structure refer to the requirements of AISC-22 [29]. The initial design results, steel sections, are shown in Table 2. The configuration of the link beam, as illustrated in Figure 6, is subsequently implemented within the EBFs frame with the load direction parallel to the main axis of the beam, as depicted in Figure 7. All of connections in the numerical models were idealized as fully welded using tie constraints to isolate the behavior of the link elements. In practice, semi-rigid connections or bolted joints with slip would introduce additional rotational flexibility and pinching effects in the hysteretic response—this is a limitation in this study. At the base of the column's, fixed support is prescribed to simulate rigid support. Meanwhile, the cyclic loading is applied at the upper ends of the columns, defined explicitly as boundary conditions (BC).

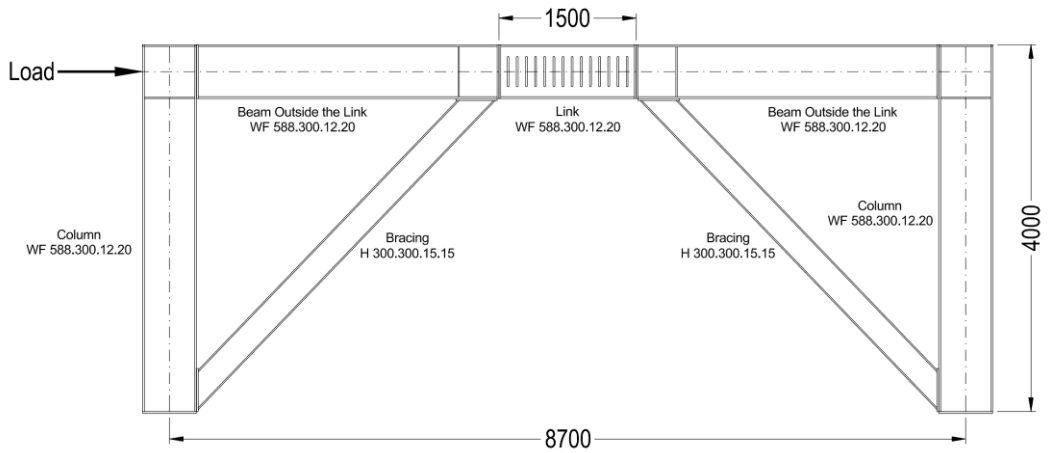

Figure 7. The EBFs frame (Unit in mm)

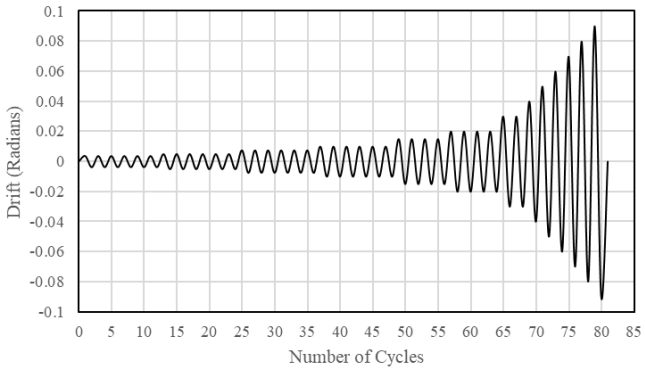

Figure 8. The loading protocol based on AISC 341-22 [30]

Table 4. The magnitude of the loading protocol based on AISC 341-22

No.	Drift ratio (rad)	Displacement (mm)	Cyclic number
1	0.00375	5.62	6
2	0.005	7.50	6
3	0.0075	11.25	6
4	0.01	15.00	6
5	0.015	22.00	4
6	0.02	30.00	4
7	0.03	44.99	2
8	0.04	59.97	1
9	0.05	74.94	1
10	0.06	89.89	1
11	0.07	104.83	1
12	0.08	119.78	1
Total cycle			**40**

The cyclic loading protocol is based on AISC 341-22 [29], which prescribes a progressively increasing drift ratio with decreasing cycle counts to simulate realistic seismic demands. As illustrated in Figure 8 and detailed in Table 4, the protocol begins with six cycles at low drift ratios (0.00375–0.01 rad), followed by four cycles at intermediate levels (0.015–0.02 rad), and culminates in single cycles at extreme drift ratios up to 0.08 rad. This sequence reflects the expected distribution of seismic energy, where structures experience numerous small deformations and fewer large excursions during strong ground motions. Displacement values corresponding to each drift level were calculated based on the link length (e = 1500 mm), ensuring accurate control of column-top displacement to achieve target link rotations. The total of 40 cycles provides sufficient resolution to evaluate stiffness degradation, strength decay, and energy dissipation across the full range of inelastic behavior. This protocol enables consistent comparison of hysteretic performance among models with varying slit geometries, while maintaining compliance with established seismic qualification standards. The assessment of the K-EBF model encompasses frame shear strength, hysteretic response, energy dissipation capacity, link failure characteristics, and overall structural ductility. Subsequently, the performance of each K-EBF frame specimen is compared, allowing the identification of the most suitable link type based on the defined evaluation criteria.

4. Results and Discussion

4.1. Stress Distribution dan Failure Mode

The numerical results for the conventional link (CV and CV-ST) shown in Figure 9(a), (b) and Figure 10(a), (b) indicate that yielding initiates at the link at a drift ratio of 0.03 rad, with stress concentrations clearly observed in the link element. As loading progresses, stress distribution extends into the beams, stiffeners, and eventually the columns, particularly at the maximum drift ratio of 0.08 rad, indicating the potential for web/flange buckling and broader plastic hinge formation. The addition of stiffeners in the CV-ST delays web buckling and increases shear demand within the link, but simultaneously transmits higher stresses to adjacent members, thereby affecting the overall strength of the system. The hysteretic displacement–force curves confirm these observations, with the CV configuration reaching a maximum force of 2832.41 kN at 61.63 mm displacement, while the CV-ST configuration achieves a slightly higher maximum force of 3223.38 kN at 61.69 mm displacement.

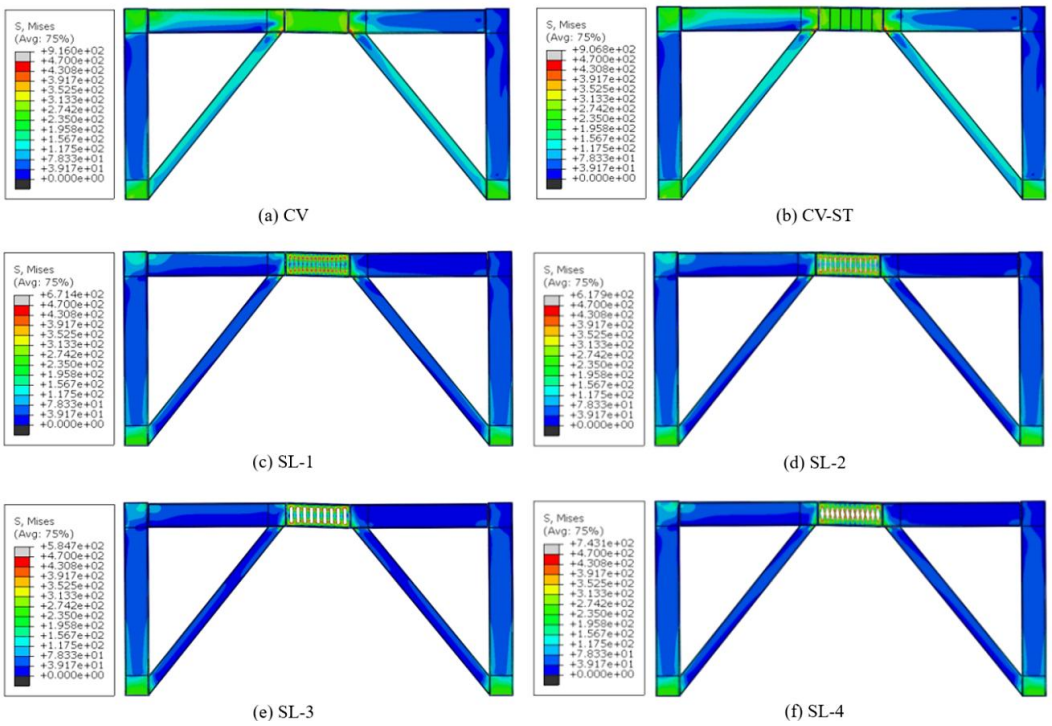

Figure 9. Stress distribution and failure mechanism in drift 0.03 radians

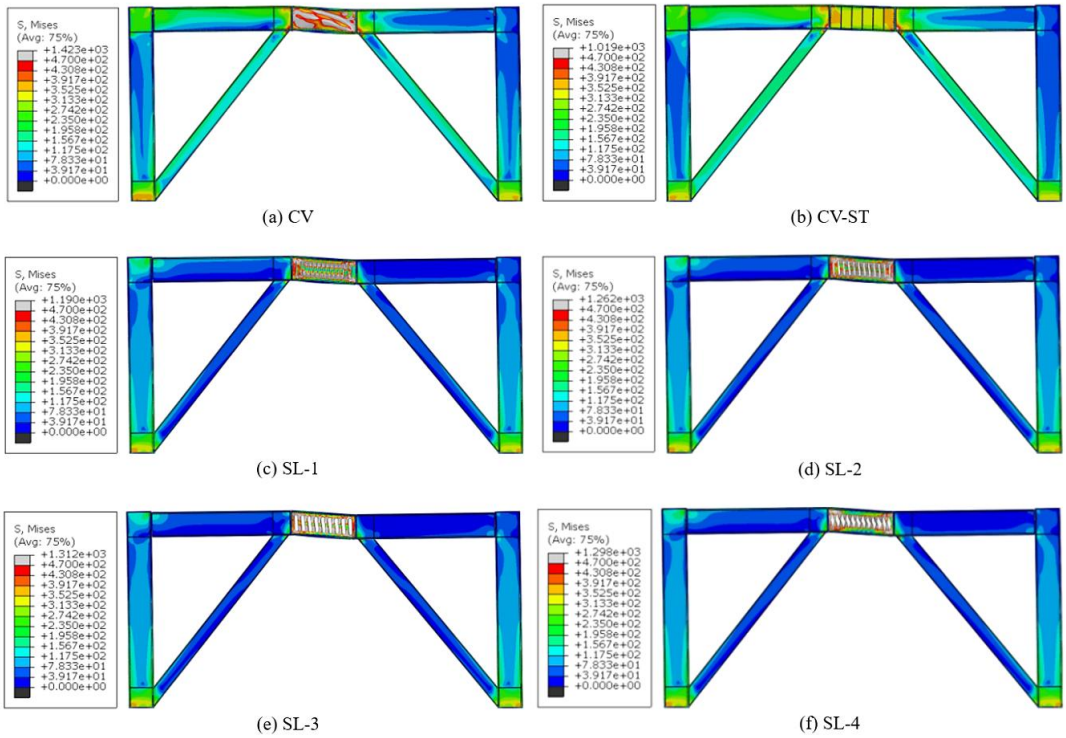

Figure 10. Stress distribution and failure mechanism in drift 0.08 radians

The slit links configuration (SL-1 to SL-4) shown in Figure 9(c), (d), (e), (f) and Figure 10(c), (d), (e), (f) demonstrate localized stress distribution confined to the slit region, consistent with the intended "structural fuse" mechanism. For SL-1 with a 20 mm slit, yielding occurs at 0.03 rad drift without significantly affecting other structural elements, and even at 0.08 rad drift the stress remains centered on the link, with a maximum force of 1357.44 kN at 61.64 mm displacement. SL-2, with a 40 mm slit, exhibits similar behavior but with a reduced maximum force of 1210.87 kN at 61.60 mm displacement. SL-3, with an 80 mm slit, shows further reduction in capacity, reaching 1051.11 kN at 59.32 mm displacement, confirming that wider slits exacerbate local strains and reduce lateral stability. Finally, SL-4, which employs a parabolic slit geometry with a diamond-shaped throat, redistributes shear more effectively and mitigates sharp stress concentrations compared to rectangular slits. This configuration sustains a maximum force of 1228.55 kN at 61.32

mm displacement, comparable to SL2, but with smoother failure progression. Collectively, these results highlight that slit link models confine damage to the link element, enhance repairability, and provide more stable hysteretic behavior, albeit at the expense of reduced peak force capacity relative to conventional link models.

For the CV and CV-ST models, yielding initiates at the link but stress progressively migrates into the beams, braces, and eventually the columns at maximum drift, indicating potential web/flange buckling and the formation of broader plastic hinges; the addition of stiffeners in CV-ST likely delays web buckling and increases shear demand within the link, though at the expense of transmitting higher demands to adjacent members. However, failure in SL-1 to SL-3 is localized within the slit region, consistent with the "structural fuse" design intent, where increasing slit width exacerbates local strains and reduces lateral stability, leading to earlier softening and diminished force capacity. The SL-4 model, with its parabolic slit geometry, redistributes shear through a diamond-shaped throat and mitigates sharp stress concentrations compared to rectangular slits, thereby supporting a smoother failure progression and sustaining slightly higher capacity than SL-2 at comparable drift. From a repairability perspective, slit links are more easily replaceable and confine damage to the link itself, whereas CV and CV-ST failures may propagate into beams and columns, necessitating multi-element repairs that increase downtime and cost.

4.2. Hysteretic Response

The hysteresis curves presented in Figure 11 illustrate the cyclic force–deformation behavior of six link configurations under repeated loading. The conventional models (CV and CV-ST) exhibit wide hysteresis loops with high peak forces, indicating substantial energy dissipation and strength capacity. CV-ST, in particular, shows enhanced loop area and peak force compared to CV, attributed to the presence of stiffeners that delay local buckling and improve shear transfer. However, both models also demonstrate stress migration into adjacent members at higher drift levels, suggesting broader plastic hinge formation and potential damage propagation beyond the link zone. The slit link models (SL-1 to SL-4) display narrower hysteresis loops with lower peak forces, consistent with their design intent as structural fuses. SL-1, with the smallest slit width, maintains relatively stable loop shapes and concentrated plasticity within the link region. As slit width increases (SL-2 and SL-3), the loops become progressively pinched, indicating reduced lateral stiffness and earlier softening. SL-4, which employs a parabolic slit geometry, shows improved loop symmetry and smoother degradation compared to rectangular slit variants, suggesting more uniform stress redistribution and enhanced deformation capacity.

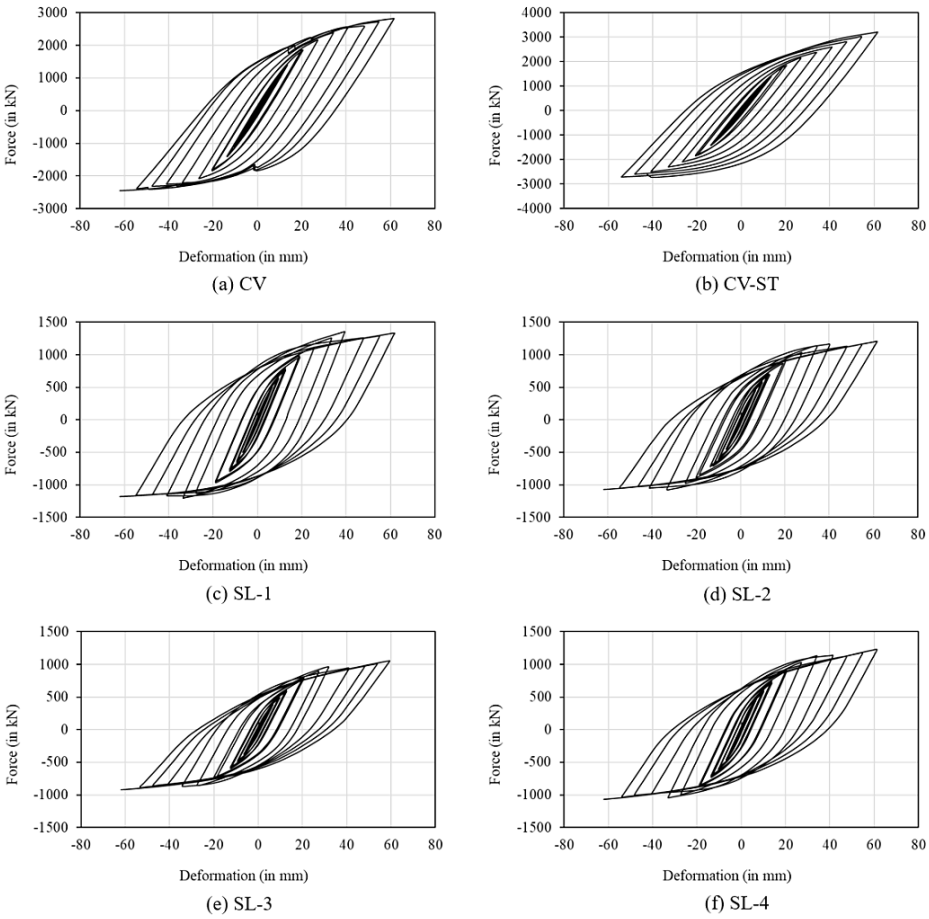

Figure 11. Hysteretic curve for each links configuration

Overall, the hysteresis behavior confirms that slit link configurations effectively confine damage within the link element, offering superior ductility and repairability at the expense of reduced strength. The conventional links, while stronger, exhibit broader stress distribution and potential damage to beams and columns. These findings support the use of slit links in seismic applications where energy dissipation and damage localization are prioritized, and highlight the importance of slit geometry in tuning cyclic performance.

4.3. Backbone Curve

The backbone curve in Figure 12 illustrates the relationship between maximum deformation and maximum force attained during each cycle of cyclic loading. This curve represents the peak response trajectory of the structure and is commonly used to evaluate strength capacity, stiffness, and ductility of the link elements. The CV and CV-ST models exhibit the highest maximum force capacity, reaching approximately ±4000 kN at ±80 mm deformation. However, both models experience more rapid stiffness degradation, as indicated by the reduction in peak force across subsequent cycles. In contrast, the slit models (SL-1 through SL-4) demonstrate lower maximum force capacity, around ±1500 kN, but maintain a more stable and consistent backbone trajectory throughout the cyclic loading.

The stability of the backbone curve in the slit models indicates that geometric modification through slit installation effectively extends the plastic zone and reduces local stress concentration, thereby enhancing ductility and resistance to cyclic degradation. This finding supports the conclusion that slit links have potential as more efficient dissipative elements in EBF systems, particularly in sustaining plastic performance under large deformations. Considering the more stable backbone trajectory and slower strength deterioration, the slit models exhibit more favorable characteristics in terms of energy dissipation and resilience under repeated cyclic loading compared to conventional models without slits.

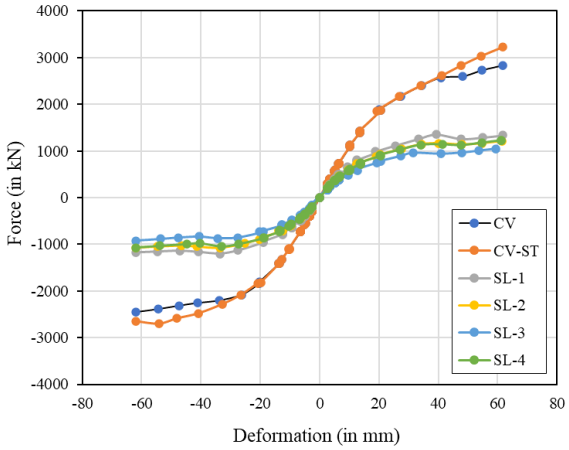

Figure 12. Comparison of backbone curve of each links configuration

4.4. Energy Dissipation

Energy dissipation is defined as the ability of structural components to absorb and release energy through inelastic deformation under cyclic or seismic loading. It is typically quantified by the area enclosed within the force–deformation hysteresis loop, representing the energy absorbed during each loading cycle [33]. The method for calculating energy dissipation uses the backbone curve (skeleton part) approach, which is the result of decomposing the hysteretic curve presented by Yue et al. (2024) [34], and Lin (2025) [35] as shown in Figure 13.

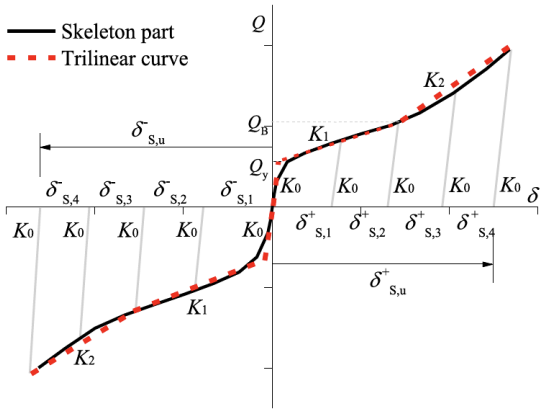

Figure 13. Decomposition of hysteretic curve to skeleton part (backbone curve)

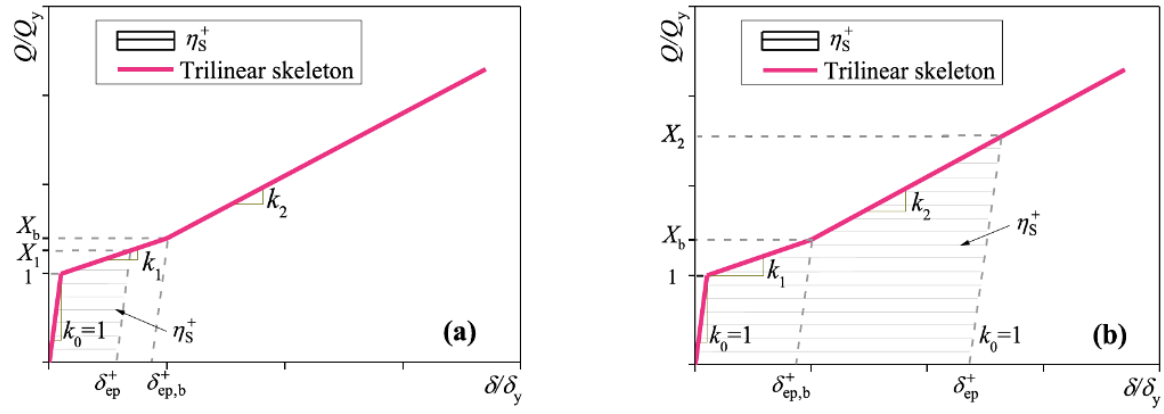

Figure 14. Energy of skeleton part in: (a) pre-buckling stage; (b) post-buckling stage

The calculation of energy dissipation for the skeleton part is divided into pre- and post-buckling stages as shown in Figure 14 with the variable of X_1 and X_2 is obtained with Equation 5 and Equation 6. By calculating the area of the shaded regions, the energy dissipation can be derived in Equation 7 and Equation 8 with δ_{ep} as the total plastic deformation, δ_{ep}^{+} as positive plastic deformation, $\delta_{ep,b}$ as total plastic buckling deformation and $\delta_{ep,b}^{+}$ as positive plastic buckling deformation.

$$X_1 = 1 + \frac{k_1 \delta_{ep}^{+}}{1-k_1} \tag{5}$$

$$X_2 = 1 + \frac{k_1 \delta_{ep,b}^{+}}{1-k_1} + \frac{k_2}{1-k_2}\left(\delta_{ep}^{+} - \delta_{ep,b}^{+}\right) \tag{6}$$

Pre-buckling stage:

$$\eta_s = 0.25\delta_{ep}\left(4 + \frac{\delta_{ep} k_1}{1-k_1}\right) \tag{7}$$

post-buckling stage:

$$\eta_s = 0.25\delta_{ep,b}\left(4 + \frac{\delta_{ep,b} k_1}{1-k_1}\right) + \left(\delta_{ep} - \delta_{ep,b}\right)\left(1 + \frac{0.5\delta_{ep,b} k_1}{1-k_1}\right) + \frac{0.25 k_2}{1-k_2}\left(\delta_{ep} - \delta_{ep,b}\right)^2 \tag{8}$$

Table 5 presents a comparative summary of energy dissipation, peak shear force, and deformation across six link configurations: CV, CV-ST, SL-1, SL-2, SL-3, and SL-4. The conventional links (CV and CV-ST) demonstrate the highest energy dissipation capacities, with CV-ST reaching 119.03 kN·m and CV 114.47 kN·m. This enhancement in CV-ST is attributed to the presence of stiffeners, which improve shear transfer and delay local yielding, thereby increasing both peak shear force (3223.38 kN) and energy absorption. Despite similar deformation levels (~61.6 mm), the stiffened configuration shows superior performance in resisting cyclic loads and maintaining structural integrity under large displacements. On other hand, the slit link configurations (SL-1 to SL-4) exhibit lower energy dissipation values, ranging from 37.95 to 58.60 kN·m, consistent with their design intent as structural fuses. SL-1, with the narrowest slit, achieves the highest energy dissipation among the slit variants (58.60 kN·m), while SL-3 records the lowest (37.95 kN·m), indicating that increased slit width reduces stiffness and energy absorption. Interestingly, SL-4, which features a parabolic slit geometry, shows improved energy dissipation (46.68 kN·m) compared to SL-2 and SL-3, suggesting that geometric optimization can partially restore performance by redistributing stress and enhancing plastic deformation.

Table 5. Comparison of the energy dissipation f all links configuration

Links configuration	Energy dissipation (kN.m)	Peak shear force (kN)	Deformation (mm)
CV	114.47	2,832.41	61.63
CV-ST	119.03	3,223.38	61.69
SL-1	58.60	1,357.44	61.64
SL-2	49.20	1,210.87	61.60
SL-3	37.95	1,051.11	59.32
SL-4	46.68	1,228.55	61.23

Overall, the results confirm that conventional links are more effective in maximizing strength and energy dissipation, making them suitable for applications requiring high resistance and limited drift. Meanwhile, slit links offer controlled damage localization and higher ductility, with energy dissipation governed by slit geometry. These findings support the strategic use of slit links in seismic design where repairability and energy absorption are prioritized over peak strength.

4.5. Ductility

Ductility is described as the capacity of a structure to sustain deformations beyond the elastic limit while maintaining stability, serving as a safeguard against brittle collapse [36]. Ductility (μ) can also be defined as the ratio between ultimate deformation (Δ_u) and the first yield deformation (Δ_y) [37], obtained from the backbone curve as shown in Figure 11, ductility can be calculated using Equation 9. The ductility values for each link configuration are shown in Table 6.

$$\mu = \frac{\Delta_u}{\Delta_y} \tag{9}$$

The comparative evaluation of the six link configurations highlights the trade-off between strength and ductility inherent in conventional versus slit link designs. The conventional specimens (CV and CV-ST) achieved the highest peak strengths, with CV reaching 2832.41 kN and CV-ST attaining 3223.38 kN, the latter representing a 14% increase due to the addition of stiffeners that enhanced shear transfer and delayed local yielding. However, their ductility ratios remained moderate, at 9.58 and 9.67 respectively, indicating that while stiffeners improve strength capacity, they do not significantly extend the deformation capacity. Stress migration into beams, stiffeners, and columns at larger drifts further suggests that conventional links are more susceptible to broader plastic hinge formation and potential damage propagation into adjacent members.

Table 6. Comparison of the ductility of all links configuration

Links configuration	F_y (kN)	Δ_y (mm)	F_{peak} (kN)	Δ_u (mm)	μ
CV	728.49	6.43	2,832.41	61.63	9.58
CV-ST	722.24	6.38	3,223.38	61.69	9.67
SL-1	411.06	5.18	1,357.44	61.64	11.90
SL-2	365.66	5.05	1,210.87	61.60	12.20
SL-3	315.08	5.02	1,051.11	59.32	11.82
SL-4	366.97	5.15	1,228.55	61.23	11.89

On the other hand, the slit link specimens (SL-1 to SL-4) demonstrated lower peak strengths, ranging from 1051.11 kN to 1357.44 kN, but consistently higher ductility ratios exceeding 11.8. This confirms that slit links are intentionally designed to sacrifice strength in favor of damage confinement and enhanced deformation capacity. Among them, SL-2 exhibited the highest ductility ratio (12.20), despite reduced strength, while the parabolic slit geometry of SL-4 redistributed shear more effectively, mitigating stress concentrations and sustaining smoother failure progression with a ductility ratio of 11.89. These results underscore the design implication that conventional links are preferable when frame-level resistance and higher base shear are prioritized, whereas slit links are more suitable for fuse-type applications where ductility, energy dissipation, and repairability are critical to seismic performance.

5. Conclusion

This study has demonstrated that slit link configurations with wide-flange (WF) sections offer a promising alternative to conventional link models in eccentrically braced frames (EBFs). Through nonlinear finite element simulations under AISC 341-22 cyclic loading, six link variants—CV, CV-ST, SL-1, SL-2, SL-3, and SL-4—were evaluated in terms of shear capacity, ductility, energy dissipation, and stress distribution. The results confirm that while conventional links (CV and CV-ST) provide higher peak shear strength and energy dissipation, they also transmit significant stress to adjacent members, increasing the risk of damage propagation. In contrast, slit links effectively confine plastic deformation within the link region, enhancing repairability and maintaining stable hysteretic behavior. Among the slit variants, SL-4 with parabolic geometry exhibited smoother stress distribution and improved cyclic stability compared to rectangular slits. These findings support the integration of slit geometries into WF profiles as a cost-effective and resilient fuse mechanism, aligning with performance-based seismic design principles and offering practical advantages for earthquake-resistant steel structures.

For future research, experimental validation is needed to complement numerical simulations, especially regarding low-cycle fatigue, fracture initiation, and Bauschinger effects. Further studies may also examine the influence of semi-rigid and bolted joints on stress redistribution and hysteretic performance. Since this study idealized all joints as fully welded, applying more realistic boundary conditions would provide results that better reflect practical applications.

6. Declarations

6.1. Author Contributions

Conceptualization, J.W.M.R., B.S., and D.I.; methodology, B.S., C.C., and D.I.; software, D.I. and A.R.A.; validation, C.C. and A.R.A.; formal analysis, B.S., D.I., and F.G.; investigation, J.W.M.R.; resources, J.W.M.R.; data curation, J.W.M.R.; writing—original draft preparation, J.W.M.R. and F.G.; writing—review and editing, B.S. and D.I.; visualization, J.W.M.R. and F.G.; supervision, C.C. and D.I.; project administration, B.S.; funding acquisition, B.S. All authors have read and agreed to the published version of the manuscript.

6.2. Data Availability Statement

The database used in the analysis is available in the article

6.3. Funding

This research is funded by the Indonesian Endowment Fund for Education (LPDP) on behalf of the Indonesian Ministry of Higher Education, Science and Technology and managed under the EQUITY Program (Contract No. 4299/B3/DT.03.08/2025 and No. 3029/PKS/ITS/2025).

6.4. Conflicts of Interest

The authors declare no conflict of interest.

7. References

[1] Keivan, A., & Zhang, Y. (2019). Seismic performance evaluation of self-centering K-type and D-type eccentrically braced frame systems. Engineering Structures, 184, 301–317. doi:10.1016/j.engstruct.2019.01.087.

[2] Mortazavi, S. J., Mansouri, I., Awoyera, P. O., & Hu, J. W. (2022). Comparison of thermal performance of steel moment and eccentrically braced frames. Journal of Building Engineering, 49, 104052. doi:10.1016/j.jobe.2022.104052.

[3] Lettieri, A., de la Peña, A., Freddi, F., & Latour, M. (2023). Damage-free self-centring links for eccentrically braced frames: development and numerical study. Journal of Constructional Steel Research, 201, 107727. doi:10.1016/j.jcsr.2022.107727.

[4] Titirla, M. D. (2023). A State-of-the-Art Review of Passive Energy Dissipation Systems in Steel Braces. Buildings, 13(4), 851. doi:10.3390/buildings13040851.

[5] Ji, X., Wang, Y., Ma, Q., & Okazaki, T. (2016). Cyclic Behavior of Very Short Steel Shear Links. Journal of Structural Engineering, 142(2). doi:10.1061/(asce)st.1943-541x.0001375.

[6] Meynerd Rafael, J. W., & Lukas, A. Y. (2020). Comparison Study of Bracing Configuration with Shear Link in Eccentrically Braced Frame Steel Structure. Journal Innovation of Civil Engineering (JICE), 1(1), 7. doi:10.33474/jice.v1i1.9058.

[7] Pangestuti, P. A., & Suswanto, B. (2021). Analisis Performa Eccentrically Braced Frames (EBF) Vertikal Link Menggunakan Wide Flange (WF) Link. Jurnal Aplikasi Teknik Sipil, 19(3), 247. doi:10.12962/j2579-891x.v19i3.9628.

[8] Mansouri, A. (2021). Development of a novel haunched link for eccentrically braced frames. Engineering Structures, 245, 112870. doi:10.1016/j.engstruct.2021.112870.

[9] Ashrafi, A., & Imanpour, A. (2021). Seismic response of steel multi-tiered eccentrically braced frames. Journal of Constructional Steel Research, 181, 106600. doi:10.1016/j.jcsr.2021.106600.

[10] Li, T., Su, M., & Guo, J. (2022). A plastic design method based on multi-objective performance for high-strength steel composite K-shaped eccentrically braced frame. Journal of Constructional Steel Research, 198, 107562. doi:10.1016/j.jcsr.2022.107562.

[11] Özkılıç, Y. O. (2022). Interaction of flange and web slenderness, overstrength factor and proposed stiffener arrangements for long links. Journal of Constructional Steel Research, 190, 107150. doi:10.1016/j.jcsr.2022.107150.

[12] Mojarad, M., Daei, M., & Hejazi, M. (2020). Optimal Design Parameters of Stiffeners for Improving Seismic Performance of Links in EBFs. International Journal of Steel Structures, 20(5), 1765–1782. doi:10.1007/s13296-020-00406-5.

[13] Al-Janabi, M. A. Q., Ün, E. M., & Topkaya, C. (2022). Development of a loading protocol for long links in eccentrically braced frames. Journal of Constructional Steel Research, 193, 107278. doi:10.1016/j.jcsr.2022.107278.

[14] Rezaee, M., & Asghari, A. (2024). Lateral-torsional buckling investigation of multi-tiers eccentrically braced frames with shear link beam. Structures, 68, 107063. doi:10.1016/j.istruc.2024.107063.

[15] Mianji, A., Garivani, S., Askariani, S. S., & Aliakbari, F. (2024). Modeling parameters and numerical acceptance criteria for steel slit dampers. Structures, 69, 107408. doi:10.1016/j.istruc.2024.107408.

[16] Askariani, S. S., & Garivani, S. (2020). Introducing and numerical study of a new brace-type slit damper. Structures, 27, 702–717. doi:10.1016/j.istruc.2020.06.019.

[17] Olia, S. S., & Saffari, H. (2024). A novel slit damper configuration to enhance ductility and seismic behavior of concentrically braced frames. Structures, 66, 106823. doi:10.1016/j.istruc.2024.106823.

[18] Gullu, A., Yuksel, E., Yalcin, C., & Buyukozturk, O. (2021). Damping effect on seismic input energy and its verification by shake table tests. Advances in Structural Engineering, 24(12), 2669–2683. doi:10.1177/13694332211010584.

[19] Hasanoğlu, S., Güllü, E., & Güllü, A. (2023). Empirical correlations of constant ductility seismic input and hysteretic energies with conventional intensity measures. Bulletin of Earthquake Engineering, 21(10), 4905–4922. doi:10.1007/s10518-023-01722-x.

[20] Katal Mohseni, P., Zahedi-khameneh, A., & Naeemifar, O. (2020). Study of the Effect of Geometric Parameters of Steel Block Slit Dampers on Energy Absorption. International Journal of Steel Structures, 20(3), 1069-1079. doi:10.1007/s13296-020-00343-3.

[21] Ahmadie Amiri, H., Pournamazian Najafabadi, E., Esmailpur Estekanchi, H., & Ozbakkaloglu, T. (2020). Performance-based seismic design and assessment of low-rise steel special moment resisting frames with block slit dampers using endurance time method. Engineering Structures, 224, 110955. doi:10.1016/j.engstruct.2020.110955.

[22] Oh, S. H., & Park, H. Y. (2022). Experimental study on seismic performance of steel slit damper under additional tensile load. Journal of Building Engineering, 50, 104110. doi:10.1016/j.jobe.2022.104110.

[23] Hwang, B. K., Kim, T. S., & Ahn, Y. H. (2023). Experimental investigation of structural behavior of 316L stainless steel and carbon steel slit dampers. Thin-Walled Structures, 186, 110704. doi:10.1016/j.tws.2023.110704.

[24] Zhou, C., Wen, H., Zhao, J., Jiang, L., Xu, X., Zheng, H., Tian, Y., Liang, M., Wang, X., & Zhang, H. (2025). Investigation of the Hysteresis Performance of Multi-Story Y-Shaped Eccentrically Bare Braced Steel Frame with Block Slit Damper (BSD). Buildings, 15(3), 451. doi:10.3390/buildings15030451.

[25] Askariani, S. S., Garivani, S., & Aghakouchak, A. A. (2020). Application of slit link beam in eccentrically braced frames. Journal of Constructional Steel Research, 170, 106094. doi:10.1016/j.jcsr.2020.106094.

[26] Montazeri, E., Kazemi, S. M., & Askariani, S. S. (2021). Finite element parametric study on the cyclic response of steel frames equipped with comb-teeth dampers. Structures, 31, 111–126. doi:10.1016/j.istruc.2021.01.083.

[27] Suswanto, B., Ghifari, F., Triwulan, Sugihardjo, H., & Pangestuti, P. A. (2025). Performance Analysis of Eccentrically Braced Frames (EBF) using Metallic Yielding Damper (MYD) with Hysteretic Steel Damper (HSD) Type. Civil Engineering Dimension, 27(1), 1–11. doi:10.9744/ced.27.1.1-11.

[28] Berman, J. W., & Bruneau, M. (2013). Overview of the Development of Design Recommendations for Eccentrically Braced Frame Links with Built-Up Sections. Engineering Journal, 50(1), 21–32. doi:10.62913/engj.v50i1.1039.

[29] ANSI/AISC 341-22. (2022). Seismic Provisions for Structural Steel Buildings. American Institute of Steel Construction (AISC), Chicago, United States.

[30] Zhuang, L. D., & Zhao, J. Z. (2022). Numerical Study on the Seismic Behavior of Eccentrically Braced Composite Frames with a Vertical Low-Yield-Point Steel Shear Link. Buildings, 12(9), 1359. doi:10.3390/buildings12091359.

[31] Musbar, J., Muhyi, A., Miswar, K., Munardy, H., & Aiyub, Z. (2023). Behavior of the Link Coupling Beam on the Eccentrically Braced Frame. Journal of Southwest Jiaotong University, 58(4). doi:10.35741/issn.0258-2724.58.4.54.

[32] Yurisman, Sari, D., Murdiansyah, L., Chairi, M., & Khadavi. (2025). Numerical Analysis of the Seismic Performance of Eccentrically Braced Frames (EBFs) in Earthquake-Resistant Steel Structures with Modified Plate Stiffener Patterns in the Link Element. Civil Engineering and Architecture, 13(4), 2895–2913. doi:10.13189/cea.2025.130407.

[33] Abduljaleel, Y. W., Ali, A. S., & Mohammed, Z. A. (2025). Energy dissipation mechanisms in reinforced concrete shear walls under seismic loading. International Journal of Advanced Technology and Engineering Exploration, 12(128), 1009–1020. doi:10.19101/IJATEE.2025.121220005.

[34] Yue, K., Xu, L., Liu, J., Fan, L., & Xu, L. (2024). Energy dissipation evaluation of butterfly-shaped steel plate shear keys under different loading protocols. Structures, 60, 105893. doi:10.1016/j.istruc.2024.105893.

[35] Lin, H.-B. (2025). Calculation of Ultimate Ductility Index Based on Hysteretic Energy Analysis of the Restoring Force Curve. Buildings, 15(17), 3152. doi:10.3390/buildings15173152.

[36] Cervera Bravo, J., & Navas-Sánchez, L. (2021). Prestress behaviour and ductility requirements in structures: solutions from a unified algebraic approach. Royal Society Open Science, 8(12). doi:10.1098/rsos.210459.

[37] da Silva, A. H. A., Tsiavos, A., & Stojadinović, B. (2023). Ductility-strength and strength-ductility relations for a constant yield displacement seismic design procedure. Bulletin of Earthquake Engineering, 21(9), 4449–4479. doi:10.1007/s10518-023-01683-1.